Acta Geochim (2021) 40(1):51–66
https://doi.org/10.1007/s11631-020-00410-w

ORIGINAL ARTICLE

Neoproterozoic highly fractionated I-type granitoids of Shillong Plateau, Meghalaya, Northeast India: geochemical constraints on their petrogenesis

Debjani Choudhury[1] · **M. Faruque Hussain**[1]

Received: 19 July 2019 / Revised: 25 February 2020 / Accepted: 6 March 2020 / Published online: 16 March 2020

Abstract There are several Pan-African granitoid plutons widely distributed in Shillong Plateau, NE India. Nongpoh (506.7 ± 7 Ma) and Mylliem (480–430 Ma) plutons were chosen for the petrological and geochemical study to constrain their petrogenesis. Nongpoh pluton consists of coarse-grained porphyritic quartz-monzogranite (NQM) and Mylliem pluton consists of medium to coarse-grained porphyritic granite (MG). The constituent minerals are K-feldspar, plagioclase, quartz, and biotite in both granitoids with accessory minerals of hornblende, zircon, sphene, and ilmenite. Both NQM and MG are metaluminous to weakly peraluminous (A/CNK = 0.82–1.06), exhibit varied ranges of SiO_2 (NQM: 58.4–64.9 wt%; MG: 66.9–69.9 wt%), and display a clear compositional gap in the Harker variation diagram. NQM contains higher abundances of CaO, MgO and $Fe_2O_3^t$ and similar K_2O and total alkali contents compared to MG. They have distinctive geochemical features typical of highly fractionated I-type granitoids such as higher abundances of K_2O, Al_2O_3, MgO, CaO, $Al_2O_3 + CaO > 15$ wt% and A/CNK < 1.1, low P_2O_5 content, enrichment in LILE, depletion in HFSE and HREE and highly fractionated REE patterns with moderate Eu anomalies, implying magma generation in a post-collisional extension setting and thinning induced asthenosphere upwelling, accompanied by the partial melting of the overlying enriched lithospheric mantle. The multi-element diagram of both NQM and MG shows pronounced negative anomalies at Ba, Nb, Sr, P, Zr, and Ti which implies a major role of crystal fractionation in their petrogenesis. High concentrations of Th, U, and Pb in the granitoid types point to additional involvement of crustal components in their generation. However, MGs with more pronounced positive spikes at U, Th, and Pb compared to NQM in multi-element diagram suggests the involvement of more felsic crustal material. The observed geochemical features of the granitoid types thus suggest that they are genetically unrelated to each other and their parental magmas were modified during magmatic differentiation processes. We suggest that the NQM and MG were formed as a result of fractional crystallization of compositionally diverse hybrid magmas produced due to mingling and mixing of an enriched lithospheric mantle-derived melts with lower crust- and middle crust-derived melts respectively during a period of extension late in the cycle of Pan-African orogeny.

Keywords I-type granitoids · Shillong plateau · Geochemistry · Petrogenesis

1 Introduction

The Shillong Plateau, a prominent Archaean gneissic complex in northeast India, has undergone a major continental crustal growth during Early Paleozoic (535–430 Ma: Yin et al. 2010; Kumar et al. 2017 and references therein) with the emplacement of voluminous granitoid plutons (viz. Mylliem, Nongpoh, Kyrdem, South Khasi). The plutons are widely distributed within the plateau as well as in the Mikir Hills massif, which is a faulted extension of the plateau lying towards the east (Fig. 1), and intruded the granite gneisses (1714–1150 Ma) and overlying Proterozoic metasediments of the Shillong Group (e.g. Majumdar and Dutta 2016). Mylliem and Kyrdem plutons are

✉ M. Faruque Hussain
faruque_geo@yahoo.co.in

[1] Department of Earth Science, Assam University, Silchar 788 011, India

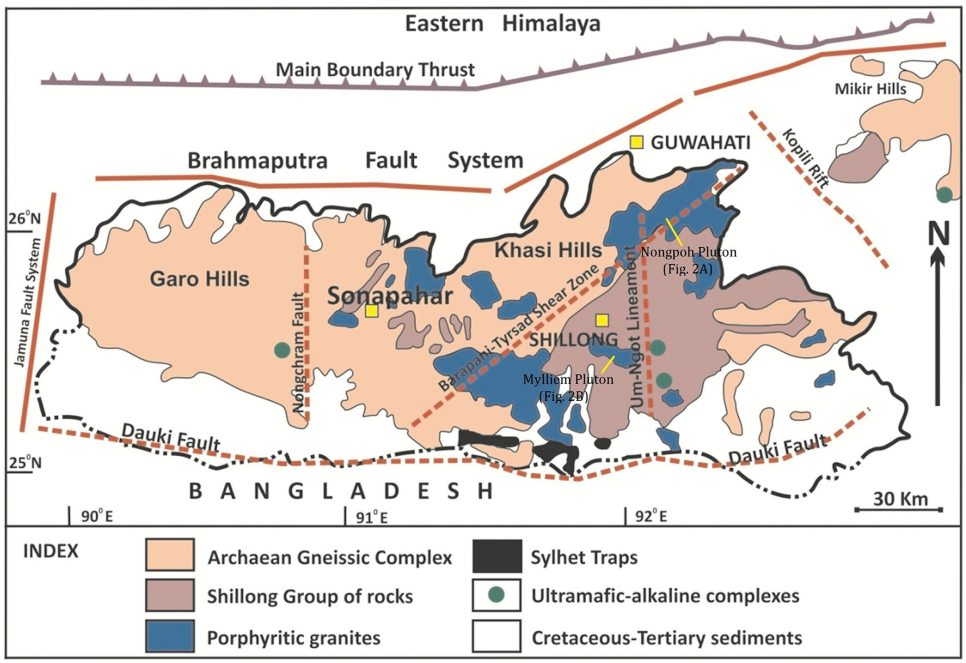

Fig. 1 Generalized geological Map of Shillong Plateau, Northeast India (modified after Srivastava and Sinha 2004)

intrusive into the Shillong Group whereas Nongpoh and South Khasi plutons intrude both the granite gneisses and the Shillong Group (e.g. Kumar et al. 2017) (Fig. 1). The granitoids of these plutons were emplaced in response to the Pan-African orogeny in the eastern Gondwana block during Neoproterozoic (Ghosh et al. 2005; Choudhury et al. 2012; Majumdar and Dutta 2016; Kumar et al. 2017). A-type granitoids linked to the Pan-African orogeny are described from Dizo valley in Mikir Hills massif (Majumdar and Dutta 2016) and Garo Hills in the western parts of the plateau (Choudhury et al. 2012). The granitoids of Nongpoh and Mylliem plutons have variable, but often high K_2O low CaO and Na_2O and P_2O_5 contents similar to I-type granite. They also contain biotite and hornblende and vary from metaluminous to weakly peraluminous as expected for highly fractionated I-type granites (Chappell and White 2001). The petrogenesis of the granitoids of the Nongpoh and Mylliem plutons were not adequately examined previously. In this paper, we present petrography and whole-rock major and trace element analyses for the granitoids for constraining the origin and evolution of the highly fractionated I-type magmatism in a post-collisional extension setting from the Shillong Plateau.

2 Geological setting

Shillong Plateau (SP) represents a Precambrian shield in northeast India, predominantly comprising of an assembly of Palaeoproterozoic basement terrain intruded by several phases of felsic and mafic magmatic rocks underlain by Shillong Group of supracrustals and overlain by Tertiary sediments. The plateau is bounded by Cenozoic faults including the Dauki fault in the south, Brahmaputra fault in the north and Jamuna fault in the west (Fig. 1). The Kopili rift in the east separates SP from the Mikir Hills (Fig. 1). The basement assembly is composed of amphibolite to granulite facies gneisses (see e.g., Nandy 2001; Bidyananda and Deomurari 2007; Majumdar and Dutta 2016; Chatterjee 2017), mafic granulites, migmatites, metapelitic granulites, and quartzo-feldspathic gneisses. The Shillong Group of rocks are of Mesoproterozoic age and are represented by a thick pile of quartzites and phyllites. Three distinct episodes of magmatic activity are identified within SP. The earliest episode is a small volume of basaltic magmatism presently represented by metadolerites (locally known as Khasi Greenstones) of Mesoproterozoic age, followed by an extensive episode of granitoid plutonism (535–430 Ma: Kumar et al. 2017; Yin et al. 2010) represented by South Khasi, Kyrdem, Mylliem, and Nongpoh plutons. The last episode of igneous activity within SP is marked by Sylhet Trap volcanism (117 Ma: Ray et al. 2005) and associated Ultramafic-Alkaline-Carbonatite (UAC) magmatism (Ghatak and Basu 2013) (Fig. 1). Tertiary sediments flank around the Plateau along its periphery with thicker piles of sediments occurring in the east and south-west (Fig. 1).

The Nongpoh pluton covers an area of $\sim$ 500 km^2 (Fig. 2a) in the northeast of SP while Mylliem pluton covers an area of $\sim$ 100 km^2 (Fig. 2b) towards the southeast of the plateau. The granitoids of both the plutons are undeformed, medium to coarse grained and porphyritic

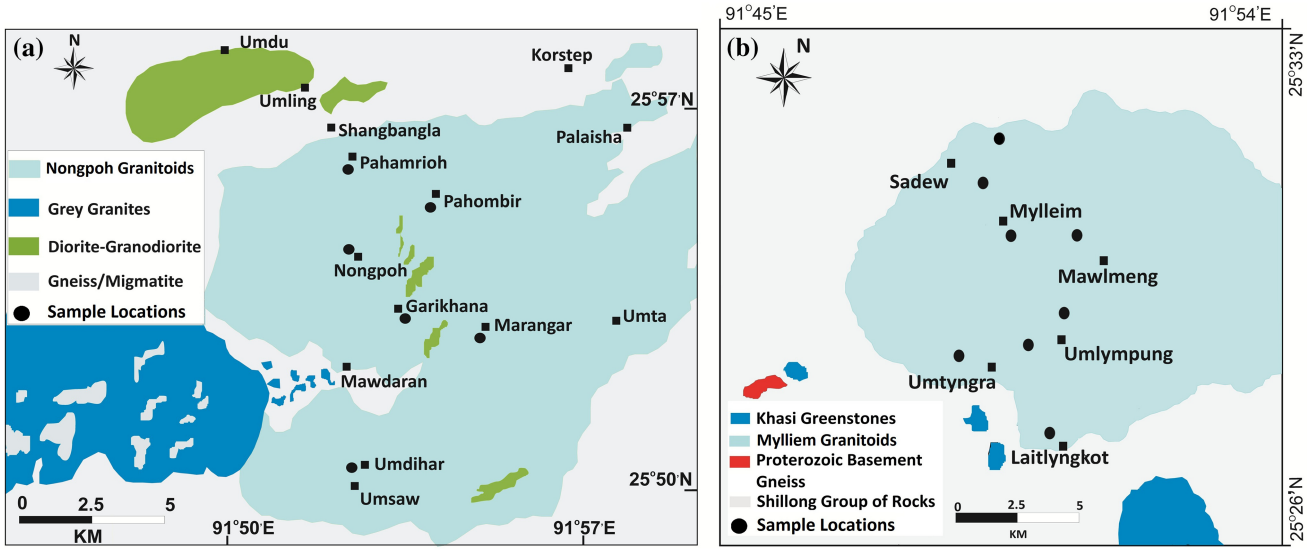

Fig. 2 Geological Map of (**a**) Nongpoh Pluton (modified after Sadiq et al. 2018) and (**b**) Mylliem Pluton (modified after Ray et al. 2011) of Shillong Plateau

in nature and contain large phenocrysts of K-feldspar (Fig. 3a, c–e). At places, the granitoids of both Mylliem and Nongpoh plutons have K-feldspar megacrysts set in equigranular groundmass. Regular occurrences of mafic microgranular enclaves (MME) of various shapes and sizes with sharp to diffuse contacts are a common feature in Mylliem granitoids (Fig. 3c, d); specks of sulfide mineralization are also observed in few outcrops. The Nongpoh granitoids are dark grey in color, coarse-grained and porphyritic in nature. Nongpoh granitoids occasionally contain xenoliths of meta-quartzite (Fig. 3a) in addition to MMEs. At places, the Nongpoh granitoids show K-feldspar phenocrysts oriented (magmatic flows) along E-W direction (Fig. 3e) indicating the presence of moderate melt-water content that imparted sufficient fluidity.

3 Analytical methodology

A large number of samples were collected along north–south traverses roughly passing through the center of the plutons. Thirty fresh granitoid samples (13 samples of Nongpoh pluton and 17 samples of Mylliem pluton) were selected for preparing thin sections following standard techniques and petrographic studies were carried out. Leica Q-win Camera and software are used for microphotography. Following petrographic studies and observations from the alteration point of view, a total of fourteen most fresh granitoid samples (8 samples of Mylliem pluton and 6 samples of Nongpoh pluton) are selected for geochemical analysis. The locations of the analyzed samples are presented in Fig. 2.

The major oxides including Loss on Ignition (LOI) are analyzed at the National Centre for Earth Science Studies (NCESS), Thiruvananthapuram, Kerala, India. The major element abundances were analyzed using WD-XRF (Bruker S4 Pioneer sequential WD X-ray spectrometer) on fused glass disks. The standards used during analysis are JG-1 and JG-2. The analytical procedures and the precision and accuracy of the analysis are as discussed in Kumar and Sreejith (2016). Trace elements including Rare Earth Element (REE) analyses of the samples were carried out at Geochemistry Laboratory, National Geophysical Research Institute (NGRI), Hyderabad, India using Inductively Coupled Plasma Mass Spectrometer (ICP-MS) (Perkin Elmer SCIEX- ELAN DRCII). The sample preparation and analytical procedures, accuracy and precision adopted during the analysis are described elsewhere (see e.g., Balaram and Rao 2003; Satyanarayanan et al. 2006). JG-2 and JG-1a are used as standards during the analysis. The detection limits for most of the trace elements including REEs were about 0.01 ng/ml and the precision is better than 6% RSD for trace and REEs. The analyzed major and trace element including REE data are presented in Table 1.

4 Petrography

The granitoids of both Nongpoh and Mylliem plutons do not show much difference in their mineralogy and textures. These are coarse-grained and porphyritic in nature and are made up predominantly of K-feldspar, plagioclase, quartz, and biotite. Prismatic microcline and lath shaped plagioclase occur as phenocrysts and display carlsbad and

Fig. 3 Photographs of the outcrops of the granitoids from Nongpoh and Mylliem plutons. (**a**) Nongpoh granitoids containing enclaves of quartzite belonging to Shillong Group of rocks, (**b**) Mylliem granitoids emplaced into the quartzites of Shillong Group of rocks. The contact area is shown with a broken yellow line. (**c**, **d**) Presence of mafic enclaves in Nongpoh and Mylliem granitoids respectively. The enclaves display sharp edges suggesting lesser chances of assimilation. (**e**) Flow bands of K-feldspars in Nongpoh granitoids, (**f**) Occurrence of a thin aplitic vein within the Nongpoh granitoids indicating another younger magmatic pulse

polysynthetic twins respectively (Fig. 4a, e). The groundmass is composed of anhedral quartz, biotite, and plagioclase with a minor abundance of hornblende and pyroxene. Sphene and zircon occur as common accessory minerals in the studied rocks; the Nongpoh granitoids additionally contain apatite and ilmenite. The granitoid samples have

Table 1 Whole-rock geochemical analyses of the granitoids from Mylliem and Nongpoh plutons of Shillong Plateau, Northeast India along with calculated CIPW normative mineralogy

Sample no	Mylliem granitoids								Nongpoh granitoids					
	M-16	M-17	M-58	M-59	M-60	M-61	M-62	M-63	N-11	N-12	N-53	N-54	N-55	N-57
Major oxides (wt%)														
SiO_2	67.8	67.1	68.9	67.3	69.9	67.6	66.9	69.4	63.1	64.9	58.4	58.6	63.6	63.3
TiO_2	0.53	0.48	0.49	0.52	0.44	0.42	0.51	0.50	0.69	0.64	1.20	1.13	0.80	0.87
Al_2O_3	15.40	15.9	15	15.89	14.7	16.2	16	14.7	17.3	16.5	15.5	16.04	16.04	15.7
MnO	0.07	0.06	0.06	0.07	0.06	0.06	0.07	0.07	0.05	0.06	0.13	0.12	0.08	0.09
$Fe_2O_3^t$	3.23	3.15	3.04	3.25	2.94	2.66	3.21	3.16	4.07	3.82	7.30	6.62	4.92	5.29
CaO	2.14	2.31	2.11	2.26	2.13	2.00	2.21	2.40	3.51	3.23	5.30	4.83	2.16	4.25
MgO	1.05	1.03	1.00	1.02	0.93	0.77	1.04	1.11	1.52	1.34	3.49	3.29	1.97	2.28
Na_2O	2.72	2.82	2.76	2.92	2.86	2.92	2.89	2.92	3.21	3.10	2.90	2.82	2.32	3.14
K_2O	5.90	6.00	5.55	5.87	4.95	6.34	6.04	4.70	5.56	5.21	4.06	5.05	6.98	3.83
P_2O_5	0.25	0.24	0.23	0.24	0.22	0.19	0.24	0.25	0.39	0.39	0.82	0.77	0.39	0.54
Total	99.09	99.09	99.14	99.34	99.13	99.16	99.11	99.21	99.4	99.19	99.1	99.27	99.26	99.29
LOI	0.55	0.52	0.46	0.53	0.51	0.52	0.55	0.47	0.42	0.39	0.49	0.45	0.38	0.38
A/CNK	1.04	1.04	1.05	1.04	1.06	1.06	1.05	1.03	0.98	0.99	0.82	0.85	1.05	0.92
A/NK	1.42	1.43	1.43	1.42	1.46	1.39	1.42	1.49	1.53	1.53	1.69	1.59	1.41	1.69
CIPW norms														
Quartz	23.9	21.9	26.2	22.10	28.9	21.4	21.3	28.4	14.4	19.1	12.6	10.4	16.9	19.3
Albite	23	23.9	23.4	24.7	24.2	24.7	24.5	24.7	27.2	26.2	24.5	23.9	19.6	26.6
Anorthite	8.98	9.89	8.97	9.64	9.13	8.68	9.40	10.3	14.9	13.5	17.3	16.2	8.17	17.5
Orthoclase	34.9	35.5	32.8	34.7	29.2	37.5	35.7	27.8	32.9	30.8	24	29.8	41.3	22.6
Corundum	1.25	1.15	1.21	1.18	1.32	1.39	1.27	1.08	0.58	0.79			1.64	
Hypersthene	2.62	2.57	2.49	2.54	2.32	1.92	2.59	2.76	3.79	3.34	8.69	8.19	4.91	5.68
Sphene											2.57	1.93		0.03
Rutile	0.45	0.41	0.42	0.44	0.37	0.35	0.43	0.42	0.63	0.57		0.21	0.71	0.76
Ilmanite	1.15	0.13	0.13	0.15	0.13	0.13	0.15	0.15	0.11	0.13	0.28	0.26	0.17	0.19
Hematite	3.23	3.15	3.04	3.25	2.94	2.66	3.21	3.16	4.07	3.82	7.30	6.62	4.92	5.29
Apatite	0.58	0.56	0.53	0.56	0.51	0.44	0.56	0.58	0.9	0.9	1.9	1.78	0.9	1.25
Trace elements (ppm)														
Sc	7.70	7.82	7.41	8.30	7.09	6.84	8.19	8.14	4.92	10.12	17.7	15.2	11.4	13.7
V	46.9	47.4	42.3	50.2	43.5	39.7	47.7	42.61	65	62.4	143	122	93.8	97.2
Cr	111	76.2	83.5	90.1	92.3	77.5	80.5	84.36	68	61.2	74.1	64.8	74.0	92.8
Co	7.59	7.16	6.55	7.47	6.58	6.31	6.76	7.11	11.4	9.86	23.3	19.2	10.5	14.02
Ni	8.28	8.38	5.99	5.15	4.54	7.98	10.1	11.84	8.70	6.24	6.18	6.21	5.44	6.56
Cu	4.91	1.10	1.50	3.86	1.15	1.69	1.39	1.54	2.26	1.77	2.14	1.90	2.59	2.23
Zn	177	9.13	13.08	127	10.71	27.22	12.61	27.96	58.8	38.0	26.6	13.2	37.2	41.5
Ga	22.1	22.4	21.4	22.98	20.7	21.8	23.4	22.7	24.9	22.3	25.4	24.5	30	24.8
Rb	303	349	341	353	316	374	363	306	174	200	169	175	263	169
Sr	306	340	294	341	285	353	327	285	912	694	826	837	621	834
Y	56.2	54.3	54.1	58.1	48.3	50.8	59.6	55.9	43.8	50.2	64.3	58.3	73.9	58.1
Zr	175	169	154	190	189	178	199	279	143	287	224	153	214	243
Nb	31.9	31.4	31.3	34.5	30.3	26.7	34.6	33.2	21.9	27.1	23	21.5	33.6	25.2
Cs	13.8	9.47	13.2	9.59	11	8.90	8.81	13.3	1.37	2.70	3.37	2.85	3.67	2.81
Ba	772	1105	875	1046	737	1149	954	745	2129	1882	1758	2188	2214	1751
Hf	6.08	5.67	5.37	6.40	6.38	6.25	6.80	8.60	4.10	8.11	6.77	4.75	6.53	7.20
Ta	3.90	6.05	3.32	5.22	3.44	3.44	4.31	3.22	2.57	2.25	0.96	0.97	3.25	2.36
Pb	188	48.2	57	142	43.6	59.8	50	57.9	40.6	36.2	30	34.2	49	37.7

Table 1 continued

Sample no	Mylliem granitoids								Nongpoh granitoids					
	M-16	M-17	M-58	M-59	M-60	M-61	M-62	M-63	N-11	N-12	N-53	N-54	N-55	N-57
Th	61.2	44.8	54.8	58.6	51.6	51.8	62.8	59.9	33	38.7	8.92	12.6	104	17.9
U	31.03	11.5	18	19.9	19.3	15.4	18.2	23.8	2.24	3.83	2.60	2.23	3.14	2.44
La	91.9	86.4	80.9	111	73.15	81.1	106	88.7	143	131	79.5	84.5	351	91.4
Ce	177	167	163	211	143	155	201	170	269	255	181	187	649	186
Pr	22.2	21.5	21.2	26	18.36	19.7	25	21.5	33.5	33.2	27.5	28.0	75.7	26.4
Nd	68.8	67.6	66.4	78.9	57.3	61.2	76.7	66.3	105	106	102	102	221	92.8
Sm	12.4	12.4	12.12	13.8	10.47	11.2	13.6	12	16.3	17.4	20.4	19.9	31.3	17.9
Eu	1.70	1.91	1.66	1.94	1.54	1.82	1.92	1.63	2.93	2.89	4.21	4.00	4.11	3.46
Gd	8.54	8.43	8.21	9.30	7.12	7.73	9.26	8.22	9.79	10.4	13.4	12.7	18.4	11.7
Tb	1.62	1.59	1.54	1.71	1.38	1.46	1.74	1.55	1.56	1.69	2.24	2.11	2.84	2.00
Dy	7.81	7.65	7.45	8.19	6.63	7.01	8.23	7.57	6.64	7.44	9.91	9.25	11.9	9.01
Ho	1.37	1.34	1.31	1.43	1.17	1.23	1.45	1.35	1.09	1.27	1.67	1.53	1.93	1.53
Er	4.30	4.18	4.12	4.48	3.70	3.83	4.56	4.20	3.09	3.81	4.87	4.41	5.47	4.40
Tm	0.73	0.69	0.69	0.74	0.62	0.65	0.77	0.72	0.44	0.61	0.72	0.66	0.79	0.66
Yb	5.25	4.94	5.00	5.32	4.62	4.61	5.47	5.28	2.87	4.13	4.79	4.27	5.08	4.18
Lu	0.87	0.79	0.81	0.87	0.76	0.77	0.90	0.87	0.43	0.67	0.74	0.67	0.75	0.67
REE	404	387	374	475	330	357	456	390	595	575	453	461	1379	452
$(La/Yb)_N$	12.6	12.5	11.6	15.0	11.4	12.6	13.9	12.1	35.7	22.8	11.9	14.2	49.6	15.7
$(La/Sm)_N$	4.8	4.5	4.3	5.2	4.5	4.7	5.0	4.8	5.7	4.9	2.5	2.7	7.2	3.3
$(Gd/Yb)_N$	1.3	1.4	1.4	1.4	1.3	1.4	1.4	1.3	2.8	2.1	2.3	2.5	3.0	2.3
Eu/Eu*	0.51	0.57	0.51	0.52	0.55	0.60	0.52	0.50	0.71	0.66	0.78	0.77	0.52	0.73
K/Ba	63.5	45.1	52.7	46.6	55.8	45.8	52.6	52.4	21.7	23.0	19.2	19.2	26.2	18.2
Rb/Ba	0.4	0.3	0.4	0.3	0.4	0.3	0.4	0.4	0.1	0.1	0.1	0.1	0.1	0.1
Zr/Nb	5.5	5.4	4.9	5.5	6.2	6.7	5.8	8.4	6.5	10.6	9.7	7.1	6.4	9.6
Ba/Rb	2.5	3.2	2.6	3.0	2.3	3.1	2.6	2.4	12.2	9.4	10.4	12.5	8.4	10.4
K/Rb	161.7	142.7	135.1	138.1	130.1	140.7	138.1	127.5	265.3	216.3	199.5	239.6	220.3	188.2

LOI loss on ignition, $Fe_2O_3^t$ total Fe expressed as Fe_2O_3

perthitic and antiperthitic textures with well-developed exsolution lamellae of plagioclase and K-feldspars respectively (Fig. 4e, f). Myrmekitic intergrowth of quartz and plagioclase is common in the studied granitoid samples (Fig. 4b, d); however, the Mylliem granitoids display a relatively higher density of the texture. Minor occurrences of sericite and chlorite are observed. In the QAP diagram (Fig. 5a) after Streckeisen (1976), all the studied Nongpoh granitoid samples plot within the field of quartz-monzonite while six Mylliem granitoid samples plot within the field of granite except for two samples which plot within the field of granodiorite (Fig. 5a), indicating higher abundance of modal quartz in the granitoids of Mylliem pluton than those of Nongpoh pluton. Further, myrmekitic intergrowths of fine crystals of quartz and plagioclase are observed more in Mylliem granitoids which might lead the point counting slightly biased towards quartz. Based on microscopic observations and QAP plot, the granitoids of Mylliem pluton are referred to as Mylliem granites (MG); while the granitoids of Nongpoh pluton are referred to as Nongpoh quartz-monzonites (NQM).

5 Whole-rock compositions

5.1 Major elements

NQMs are less siliceous (SiO_2 = 58.4–64.9 wt%) than MG with much higher SiO_2 (66.9–69.9 wt%). NQM however, has the higher concentrations of CaO, MgO, Al_2O_3 and Fe_2O_3 than MG; but they have similar abundances of K_2O (MG = 4.7 to 6.34 wt%; NQM = 3.83–6.98 wt%), and

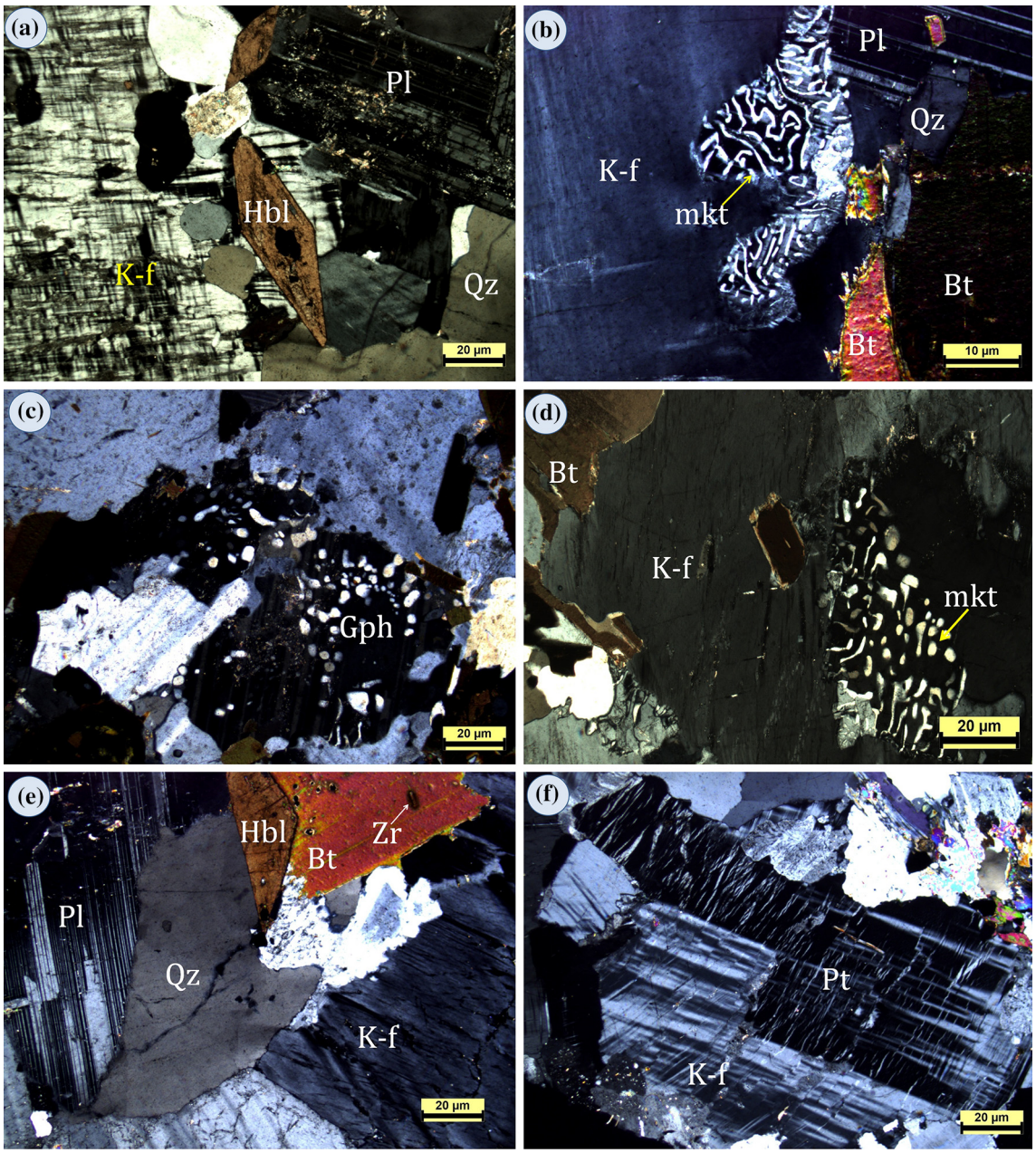

Fig. 4 Photomicrographs of the granitoids of Nongpoh and Mylliem Plutons under cross-polarized light. The Nongpoh granitoids show hypidiomorphic (**a**). myrmekitic (**b**). and graphic textures (**c**). The Mylliem granitoids show myrmekitic (**d**). hydidiomorphic (**e**). and perthitic (**f**). textures. Mineral abbreviations: Pl: plagioclase; Pt: microcline perthite; Qz: quartz; Bt: biotite; K-f: K-feldspar; Hbl: hornblende; Zr: zircon; Gph: graphic texture; mkt: myrmekitic texture

average total alkalis ($K_2O + Na_2O$: NQM = 8.03 wt%; MG = 8.52 wt%). A clear compositional gap between NQM and MG in many major elements is observed in Harker variation diagrams (Fig. 6a). The alumina saturation index A/CNK [= $Al_2O_3/(CaO + Na_2O + K_2O)$, mol] values of MG ranges between 1.03 and 1.06 and exhibit weakly peraluminous characteristics (Fig. 7b). The NQM samples with A/CNK values ranging between 0.82 and 1.05 are transitional from metaluminous to weakly peraluminous (Fig. 7b). In the Harker variation diagrams, (Fig. 6a), the NQM samples show a negative correlation for $Fe_2O_3^t$, CaO, P_2O_5, TiO_2, MnO and MgO against SiO_2 except for Al_2O_3, Na_2O and K_2O which plot scattered (Fig. 6a). By contrast, MG samples display sharp negative correlations of Al_2O_3 and K_2O contents against SiO_2, while other oxides show clustered plots against SiO_2 with no definite trends (Fig. 6a). In the normative Ab-An-Or diagram (O'Connor 1965; Barker 1979) the studied samples of

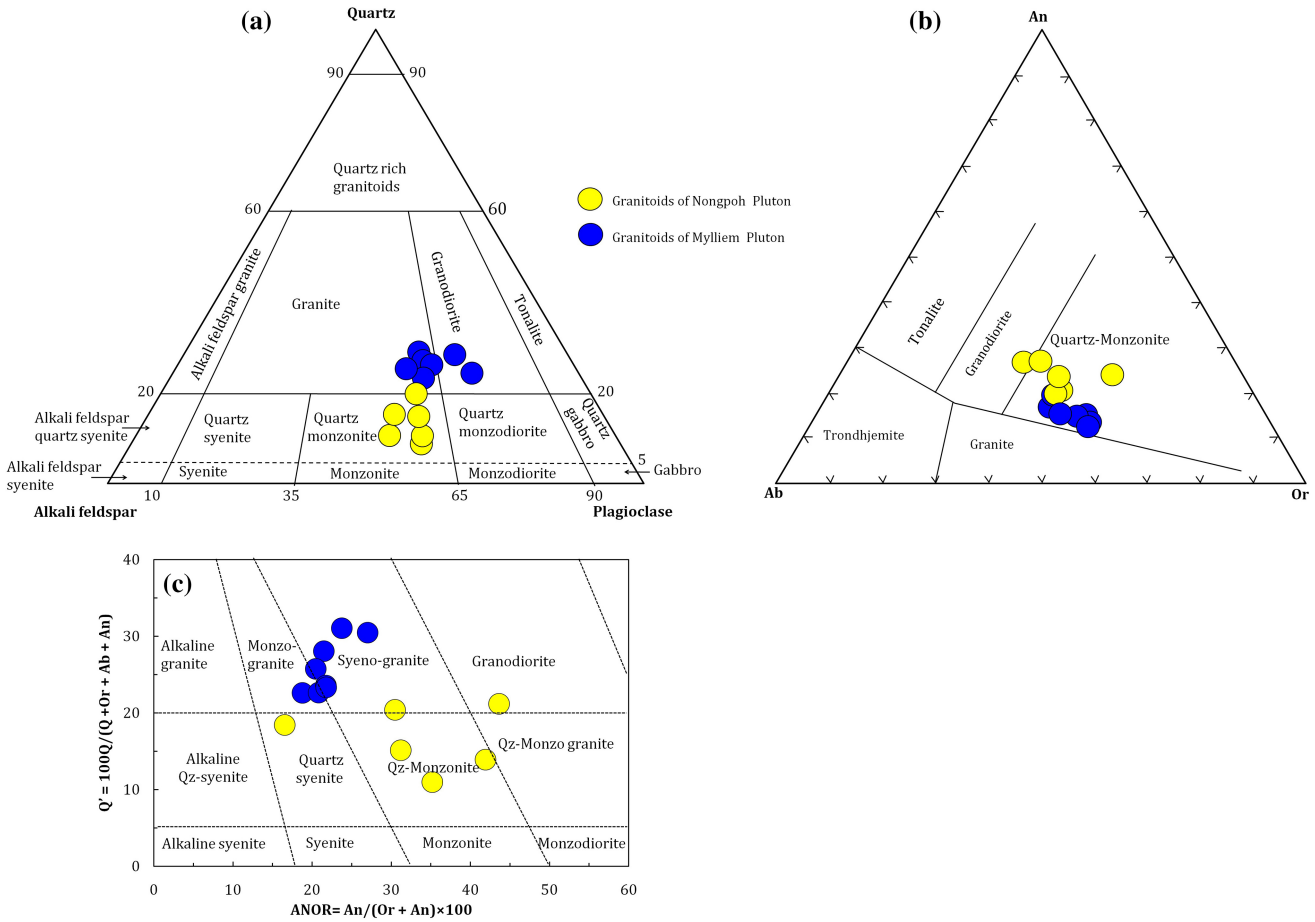

Fig. 5 (**a**) IUGS modal (after Streckeisen 1976), (**b**) Normative An–Ab–Or (after O'Connor 1965; Barker 1979) and (**c**) normative Q′-ANOR (after Streckeisen and LeMaitre 1979) classification diagrams of the granitoids of Nongpoh and Mylliem Plutons

NQM predominantly plot within the field of Quartz-Monzonite except for one sample which plots on the boundary with Granodiorite (Fig. 5b). The samples of MG, however, plot along the boundary between Quartz-Monzonite and Granite fields (Fig. 5b). In the Q-ANOR diagram (Fig. 5c) the MG samples plot within the field of Granites (Syeno-granite and Monzogranite), while NQM samples plot from Quartz-Syenite through Quartz-Monzonite to Granodiorite fields. Based on the modal QAP diagram (Fig. 5a), normative Or-Ab-An diagram (Fig. 5b); Q-ANOR diagram (Fig. 5c), A/CNK versus A/NK diagram (Fig. 7b) and SiO_2 versus ($Na_2O + K_2O$)–CaO diagram (Fig. 7a), MG may be defined as high-K, alkali-calcic, and weekly peraluminous granites and the NQM may be defined as high-K, alkali-calcic, metaluminous to weekly peraluminous quartz-monzonites.

5.2 Trace elements

Both NQM and MG samples are enriched in large ion lithophile elements (LILEs) (Rb, Sr, Ba) and high field strength elements (HFSEs) (Zr, U, Th, Y, and Ga). The Harker variation diagrams for the selected LILEs (Rb, Ba, Sr) and HFSEs (Zr, Nb, Th, Ga, U) of the studied granitoids are plotted against SiO_2 (Fig. 6b). MG samples show a nearly perfect negative correlation for Rb, Ba, Zr, Nb, and Ga; positive correlation for U, a mild negative correlation for Sr against SiO_2, however, Th does not show any definite trend (Fig. 6b). By contrast, the NQM samples display mild positive correlation trends for Rb, Th, and Nb and strong negative correlation for Sr and Ga against SiO_2 (Fig. 6b).

Primitive mantle (PM) normalized (PM values after Sun and McDonough 1989) multi-element variation diagram for all the studied granitoids displays enriched and fractioned patterns with LILEs enriched up to 60–700 times PM and HFSEs up to 8 to 30 times PM and negative anomalies at Ba, Nb, Ce, Sr, P, Zr and Ti indicating fractionation of feldspar, apatite and Fe-Ti oxides (Fig. 8). NQM samples show distinctive enrichment of LILEs like Ba, La, Ce, Sr and Nd and HFSEs like Pr Sm, Eu, Ti, P, and Dy compared to MG (Fig. 8). The MG samples,,

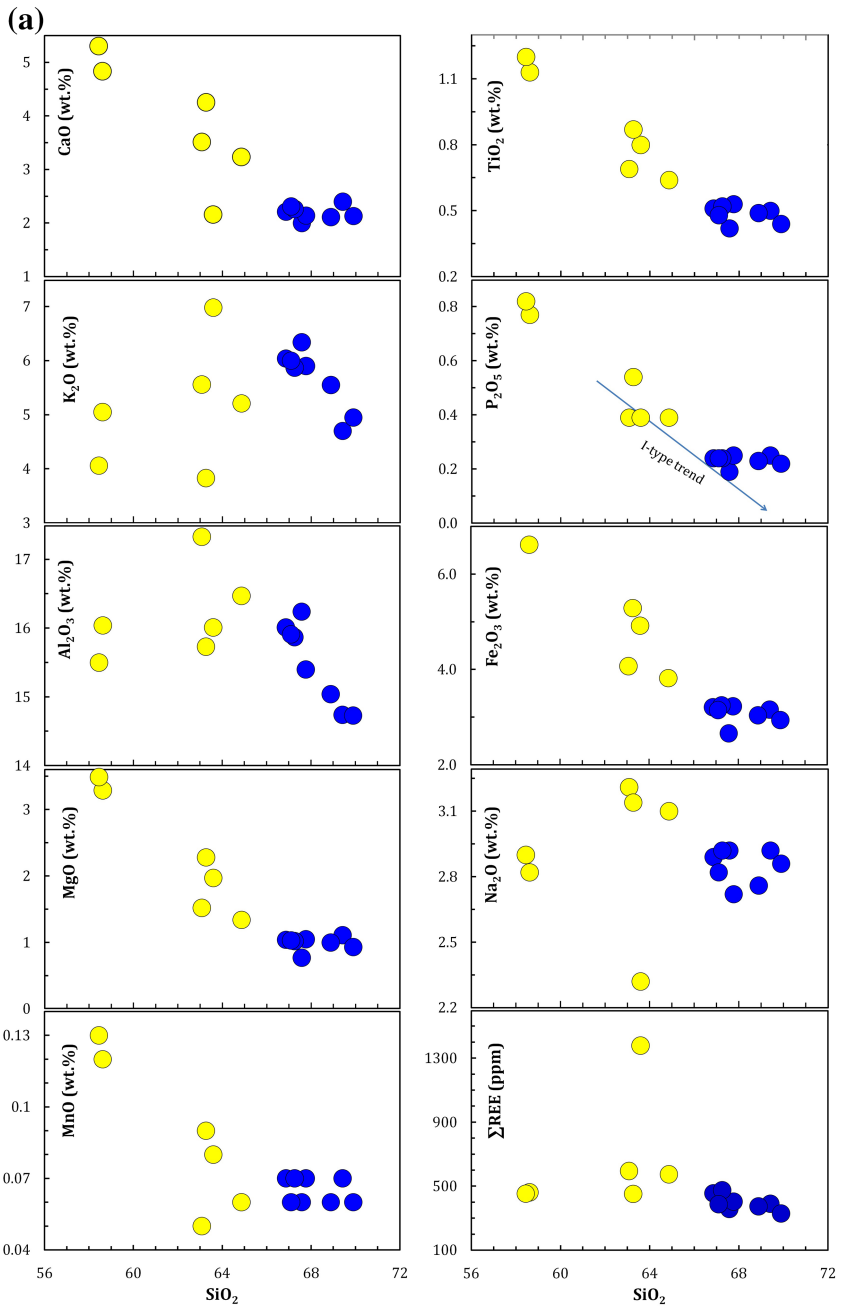

Fig. 6 Harker variation diagrams for selected (**a**) major oxides and (**b**) trace elements for the Nongpoh and Mylliem granitoids. Symbols are as used in Fig. 5

however, show enrichment of HFSEs like Nb, Ta, Yb, and Lu compared to NQM and display positive anomalies in Rb, Th, U, and Pb (Fig. 8). The NQM samples are characterized by higher total rare earth elements (REE) content ($\sum$REE = 452–596 ppm) compared to those of MG ($\sum$REE = 330–475 ppm). One NQM sample (N-55) has conspicuously high REE abundance of 1379 ppm. in the Harker variation diagram, MG samples show a gentle negative correlation between total REE ($\sum$REE) and SiO_2 but, NQM samples plot scattered (Fig. 6a). The chondrite normalized REE patterns for all the studied samples are enriched and strongly fractionated with light REE (LREE) enrichment and heavy REE (HREE) depletion. The LREE enrichment of the MG and NQM samples are almost similar and are of the order of 300–700 times chondrite while HREEs of MG and NQM samples are of the order of 30 to 40 times and 15 to 20 times chondrite respectively. The samples of NQM exhibit strongly fractionated REE patterns [$(La/Yb)_N$ = 11.9–35.7], associated with more fractionated LREEs ($(La/Sm)_N$ = 2.5–5.7) and un-fractionated (relatively flat) HREE's [$(Gd/Yb)_N$ = 2.1–3.0] (Fig. 9). The sample N-55 displays a highly erratic fractionated pattern with $(La/Yb)_N$ = 49.6. The MG samples, however, display relatively lesser degree of fractionation

Fig. 6 continued

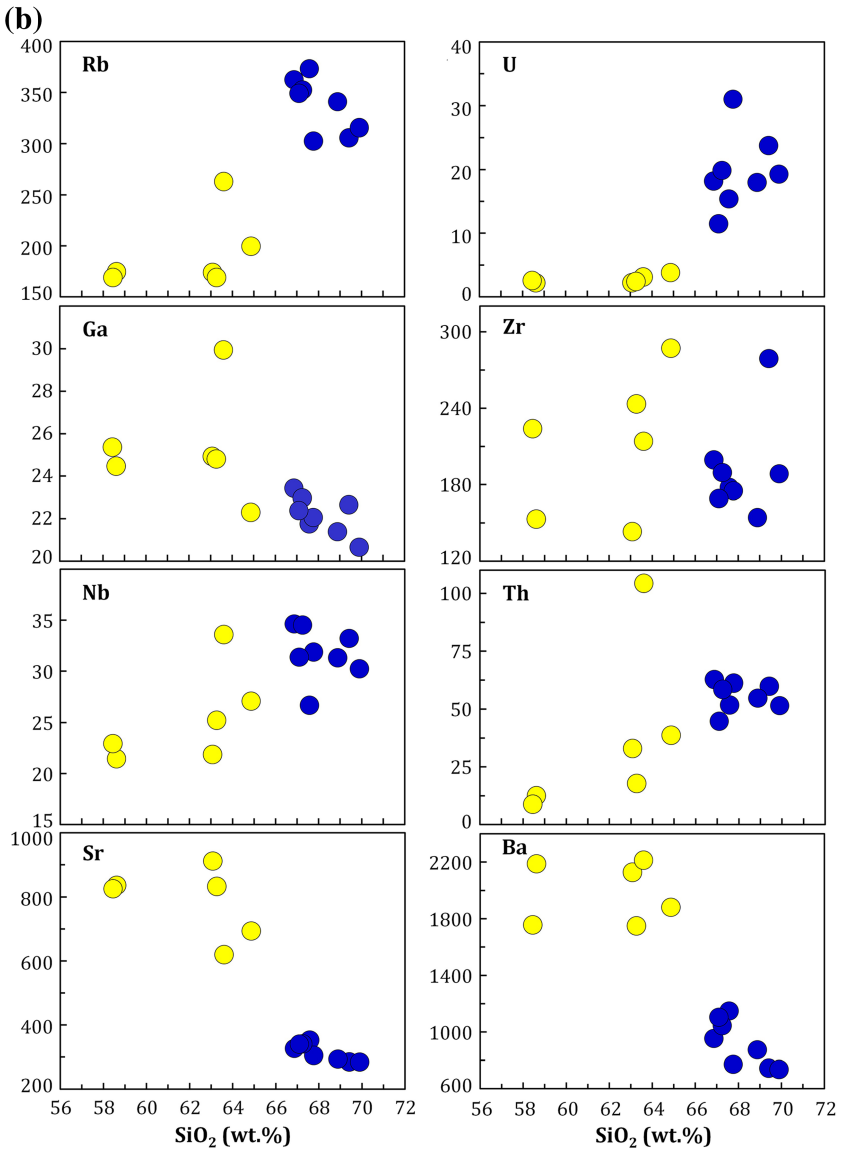

with $(La/Yb)_N$ ratios ranging from 11.4 to 15.0, associated with less fractionated LREEs [$(La/Sm)_N$ = 4.3–5.2] and more fractionated HREEs [$(Gd/Yb)_N$ = 1.3–1.4] than NQM samples (Fig. 9). On the REE patterns, strong negative Eu anomalies (Eu/Eu*: NQM = 0.52–0.78; MG = 0.50–0.60) are evident for all the studied samples.

6 Discussions

6.1 Geochemical classification

Both MG and NQM samples display magnesian character and occur conspicuously within the field of I-type granites in the FeO*/(FeO* + MgO) versus SiO_2 discrimination diagram of Frost et al. (2001) (Fig. 7c). In the ($Na_2O + K_2O$-CaO) versus SiO_2 plot of Frost et al. (2001), the studied granitoids show predominantly alkali-calcic affinity and occur within the field of I-type granitoids (Fig. 7a). In the Molar A/NK versus A/CNK plot (after Chappel and White 1992), all the samples of NQM and MG show metaluminous to weakly peraluminous nature (A/CNK < 1.1) (Fig. 7b). Therefore the studied NQM and MG samples with lower SiO_2 and $Na_2O + K_2O$ content (< 9 wt%) (subalkaline), lower FeO*/Feo* + MgO (magnesian), K_2O/Na_2O (avg: NQM = 1.80, MG = 1.98), and TiO_2/MgO (avg: NQM = 0.40, MG = 0.49) ratios; remarkably higher abundances of Al_2O_3, MgO and CaO, $Al_2O_3 + CaO > 15$ wt% and A/CNK < 1.1, typically exhibit the major element characteristics of highly fractionated I-type granitoids (e.g. Chappell 1999; Chen et al. 2000; Wu et al. 2003a,b; Li et al. 2007; Qiu et al. 2008; Zhu et al. 2009; Tao et al. 2013). The studied granitoids show decreases in P_2O_5 when SiO_2 contents are high (Fig. 6a), which is

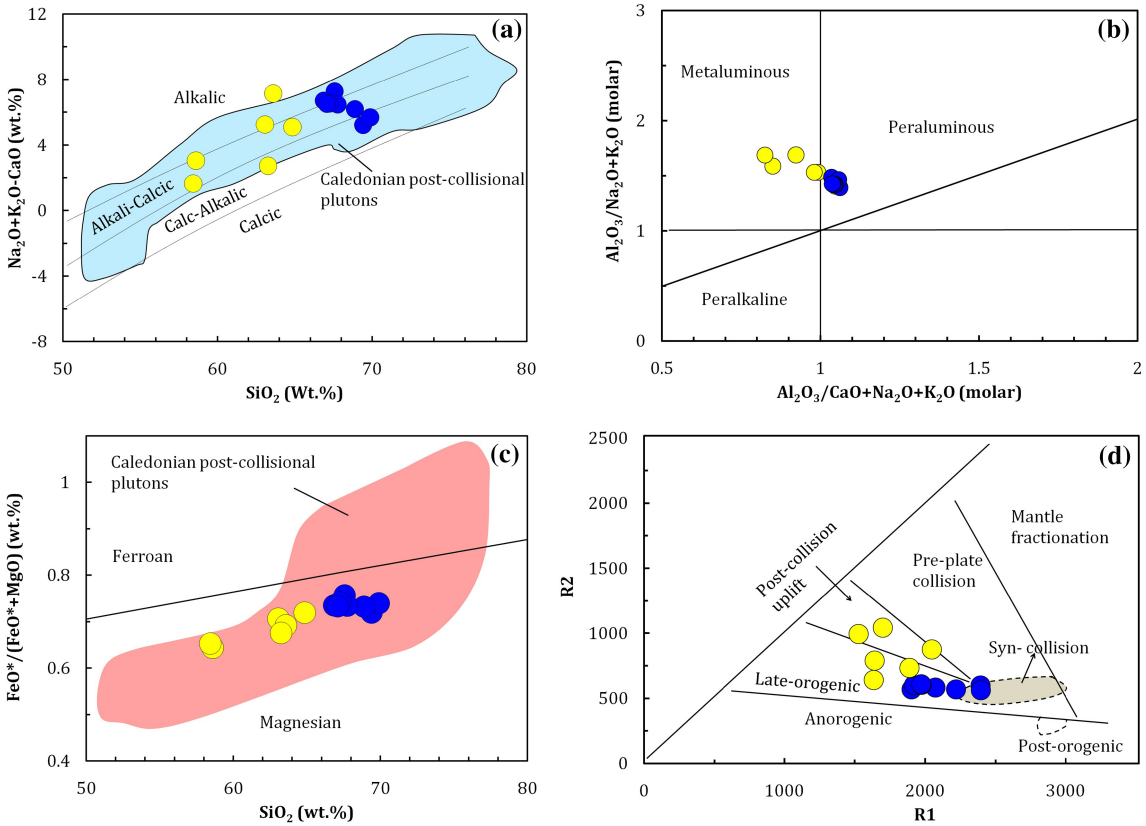

Fig. 7 Discrimination diagrams for the granitoids the Nongpoh and Mylliem plutons (**a**) $Na_2O + K_2O$–CaO versus SiO_2 diagram (after Frost et al. 2001); (**b**) molar $Al_2O_3/(Na_2O + K_2O)$ versus molar $Al_2O_3/(CaO + Na_2O + K_2O)$ diagram (after Chappel and White 1992); (**c**) FeO*/(Feo* + MgO) versus SiO_2 (after Frost et al. 2001) and (**d**) R1[4Si–11(Na + K)–2(Fe + Ti)]–R2 [6Ca + 2 Mg + Al) multicationic diagram (after de la Roche et al. 1980 and later modified by Batchelor and Bowden 1985). Symbols are as used in Fig. 5

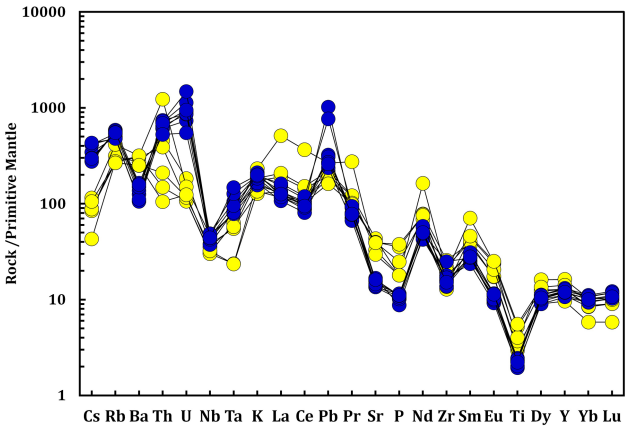

Fig. 8 Primitive mantle-normalized multi-element variation diagram for the Nongpoh and Mylliem granitoids. Primitive mantle values are after Sun and McDonough (1989). Symbols are as used in Fig. 5

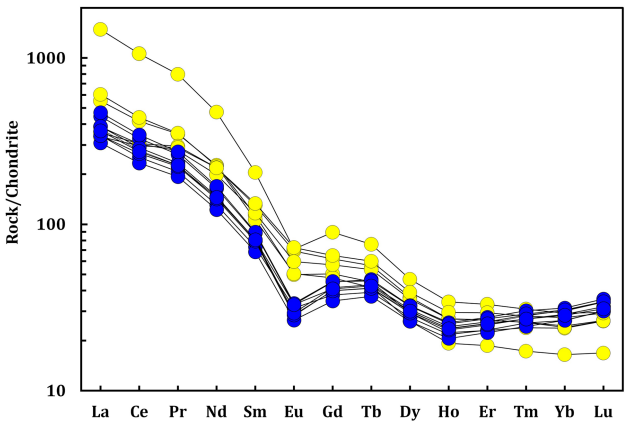

Fig. 9 Chondrite-normalized REE patterns for granitoids of Nongpoh and Mylliem plutons. The normalization values are from Sun and McDonough (1989)

considered an important distinguishing feature of I-type granites from S-type granites (Wolf and London 1994). Apatite reaches saturation in metaluminous and weakly peraluminous melts (A/CNK < 1.1) but remains highly soluble in strongly peraluminous melts and is successfully used in many studies (e.g. Chappell 1999; Li et al. 2003; Wu et al. 2003a). The trace elemental characteristics of the granitoids including depletion of Nb, Ta, Ti, Ba, Sr, and P and enrichment of Rb, Th, and U also point to their fractionated I-type affinity. The trends of increase in Th and Y against increasing Rb for MG and NQM samples (Fig. 10a,

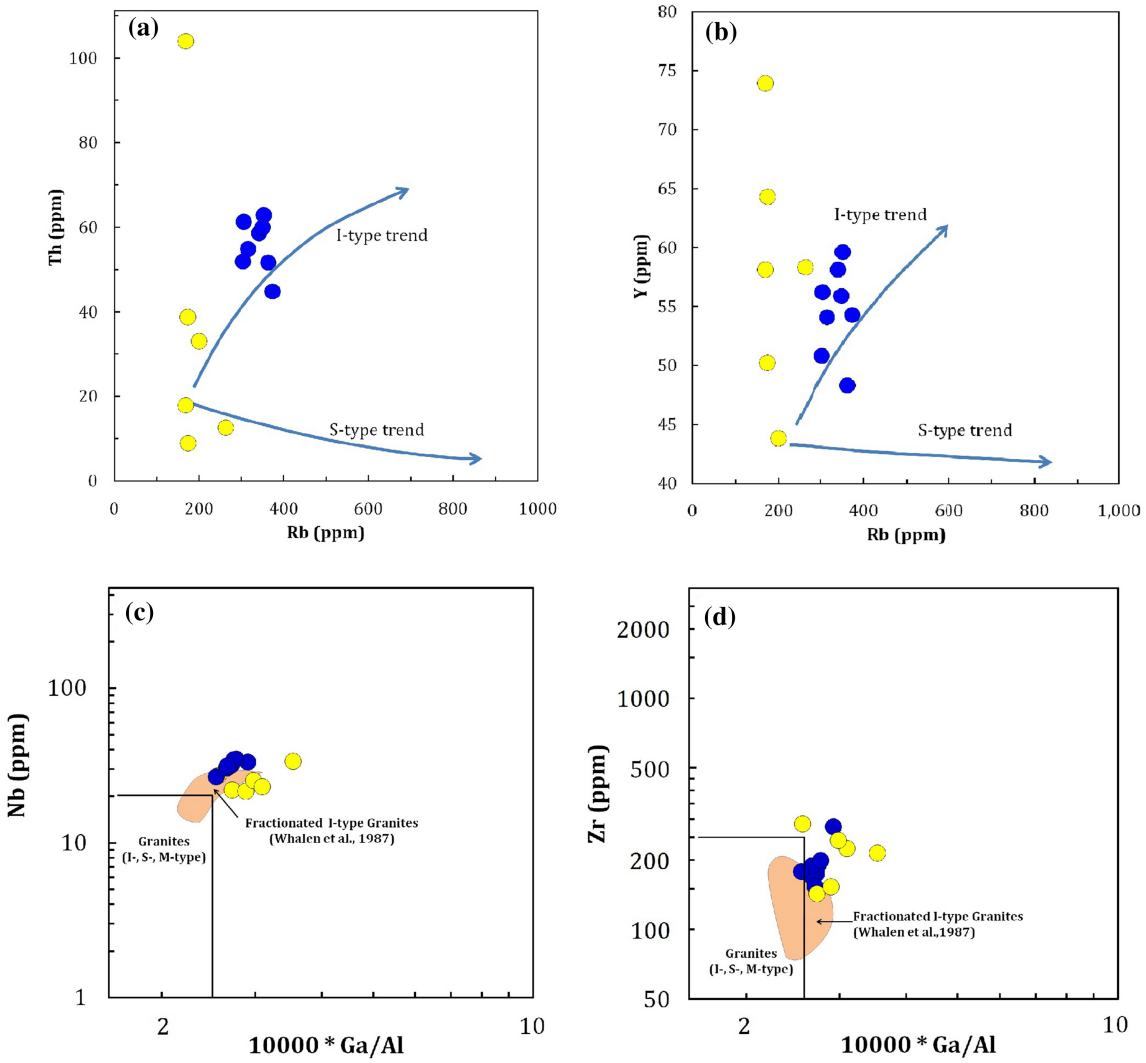

Fig. 10 Trace element classification diagrams (**a**) Th (ppm) versus Rb (ppm) and (**b**) Y (ppm) versus Rb (ppm) (after Li et al. 2007), (**c**) Nb (ppm) versus 10,000* Ga/Al, and (**d**) Zr (ppm) versus 10,000 Ga/Al (after Whalen et al. 1987) for the Nongpoh and Mylliem granitoids. Symbols are as used in Fig. 5

b), also conform to the typical I-type granite evolution trend. Furthermore, the studied granitoids plot around the fractionated I-type field in the Nb versus 10,000*Ga/Al and Zr versus10,000*Ga/Al plots of Whalen et al. (1987) suggesting their fractionated I-type affinity (Fig. 10c, d). Thus, we consider the studied NQM and MG samples are of highly fractionated I-type granitoids.

6.2 Petrogenesis

Both Nongpoh and Mylliem plutons were emplaced by independent magmatic pulses which are evident from their crystallization ages of 506.7 ± 7 Ma (Kumar et al. 2017) and Ca. 480 to 430 Ma (Yin et al. 2010) respectively. The petrographic and geochemical characteristics of the NQM and MG samples as described above are consistent with those of highly fractionated I-type granitoids, genetically unrelated to each other. To constrain the petrogenesis of highly fractionated I-type granites, several processes are hypothesized including: (a) differentiation of mantle-derived mafic magma (Chiaradia 2009; Li et al. 2009); (b) partial melting of a mixed source rock produced by intercalation of underplated mafic magma in lower crustal rocks (Wu et al. 2003a,b; Li et al. 2007), and (c) mixing of mantle- and crustal derived magmas, which, in turn, underwent fractional crystallization (Chen et al. 2000; Kemp et al. 2005; Qiu et al. 2008; Zhu et al. 2009; Tao et al. 2013). The Harker variation diagrams for major oxides and trace elements against SiO_2 for the NQM and MG samples display a clear compositional gap which suggests the granitoid types were evolved from compositionally different magma. The major oxide data including

the SiO_2, MgO, CaO and Al_2O_3 contents of the studied granitoids suggest that the NQM samples were derived from a less evolved magma while MG samples were derived from a strongly evolved magma. In general, the samples of MG and NQM display enriched LILEs and LREEs, depleted HFSE and HREE and pronounced negative anomalies at Ba, Nb, Ti, and Ta, Eu (Figs. 8, 9). The extreme enrichment of incompatible elements in both the granitoid types may arise from the partial melting of an enriched lithospheric mantle source metasomatised during a previous subduction event prior to melting (Chakrabarti et al. 2007; Sami et al. 2017). Higher values of K/Ba and Rb/Ba and significantly lower values of Zr/Nb, Ba/Rb and K/Rb, in the MG samples compared to those of NQM samples, indicate that MG has undergone stronger fractionations of plagioclase and K-feldspar compared to NQM. Similar observations are also made from the Multi-elemental diagram where the samples of MG display more pronounced negative anomalies at Eu, Ba, Ta, Nb, Sr, P, Zr, and Ti compared to the samples of NQM (Fig. 8), reflecting higher degrees of fractionation of plagioclase, K-feldspar, apatite, zircon and Fe-Ti oxides from the MG magma and a lesser degree of fractionation of these phases from the NQM magma. It thus appears that crystal fractionation was one of the most important magma modifying process for the studied granitoid types. In addition to fractional crystallization mixing with crustal melts also appears to be a dominant process in the magmatic evolution of the granitoids. High concentrations of Th (NQM: 8.9–104 ppm; MG: 44.8–62.8 ppm), Pb (NQM: 30–49 ppm; MG: 43.6–188 ppm) and U (NQM: 2.23–3.83 ppm; MG: 11.5–31 ppm), clearly indicate involvement of crustal materials, although of varied compositions, for the magmatic evolution of NQM and MG. MG samples display more pronounced U, Th, and Pb positive spikes compared to the NQM samples (Fig. 8) suggesting the involvement of more felsic crustal material in their source magma. Occasional occurrences of MMEs in Nongpoh pluton against higher occurrences of MMEs in Mylliem pluton additionally suggest that magma mixing may have played some role in the petrogenesis of the granitoids of both the plutons. Consequently, the geochemical variation in the granitoids of both the plutons can be explained by fractional crystallization coupled with the mixing of crustal melts. We, therefore, consider that the parental magma for both the plutons are linked to a post-collisional lithospheric extension and thinning, which caused an upwelling of the hot asthenospheric mantle and in turn induced partial melting of the overriding enriched lithospheric mantle. Parental magma for the granitoid types can also be produced through partial lithospheric delamination and upwelling of the hot asthenosphere, causing extensive melting of the subcontinental mantle lithosphere (e.g. Avigad and Gvirtzman 2009; Farahat et al. 2011). The Nongpoh pluton was most likely formed by strong fractional crystallization of a hybrid magma formed due to mingling and mixing of both mantle-derived melts and melts of lower crustal melting triggered by underplating of mantle melts. Mylliem Pluton, however, was emplaced later to Nongpoh Pluton and bears more evolved and felsic-crustal signatures. It was probably formed by extensive fractional crystallization of a hybrid magma with both mantle-derived melt and melt of middle crustal melting due to interaction with hot ascending magmas and decompression driven by crustal thinning during the extensional stage.

6.3 Tectonic setting

In the Rb versus Y + Nb and Nb versus Y tectonic discrimination diagrams of Pearce et al. (1984) the samples of NQM and MG appeared to be within plate granites (WPG) (Fig. 11a, b) and occur conspicuously within the field of Post-collisional granitoids of Pearce (1996) (Fig. 11a). In the FeO*/(FeO* + MgO) versus SiO_2 (Fig. 7c) and ($Na_2O + K_2O$–CaO) versus SiO_2 plots (Fig. 7a), the NQM and MG samples plot well within the compositional fields of Caledonian post-collisional or post–orogenic granitoids (fields after Frost et al. 2001). The dominantly post-collisional nature of the studied samples as revealed from the plots of Pearce (1996) and Frost et al. (2001) are also consistent with the inferences drawn from the R1–R2 multi-cationic diagram of de la Roche et al. (1980) (modified by Batchelor and Bowden 1985) in which the MG samples plot in the field of late-orogenic group, while the NQM samples plot within the fields of late-orogenic to post-collision uplift granite group (Fig. 7d). We, therefore, consider that the studied granitoids of Nongpoh and Mylliem plutons were generated in post-collisional extension setting following the collision of India, Australia and Antarctica during the assemblage of the Eastern Gondwana landmass.

6.4 Geodynamic implications

Several studies on the formation of Gondwana supercontinent suggest that the final amalgamation of east- and west- Gondwana landmasses at around 620–520 Ma followed by the closure of the Mozambique Ocean, resulting in Pan-African orogenies (Meert and Van der Voo 1997; Kroner et al. 2000; Collins and Windley 2002; Meert 2003; Abdel-Rahman 2019). East Gondwana landmasses were comprised of an ill-defined collage of continental blocks represented by India, Seychelles, Sri Lanka, Madagascar, East Antarctica, and Australia and west Gondwana landmasses comprised of Africa and South America.

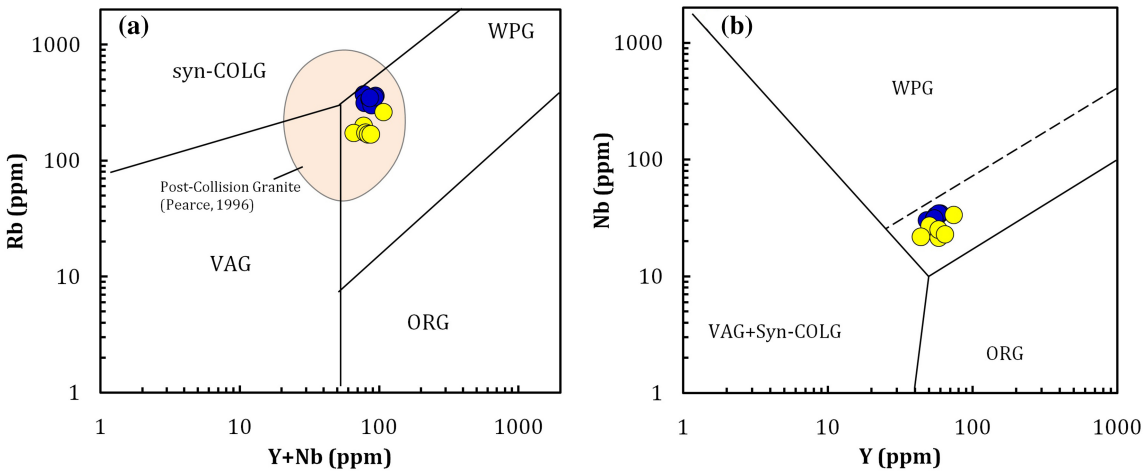

Fig. 11 (**a**) Rb versus Y + Nb and (**b**) Nb versus Y tectonic discrimination diagrams (after Pearce et al. 1984) for the granitoids from Nongpoh and Mylliem plutons of Shillong Plateau. Symbols are as used in Fig. 5. VAG: volcanic arc granites; ORG: ocean ridge granites; WPG: within plate granites; syn-COLG: syn-collision granites

Magmatism related to extensional setting within several Pan-African domains across the world including Arabian Nubian Shield, southern Madagascar, southern India, Sri Lanka and part of Dronning Maud Land in Antarctica during the amalgamation between East and West Gondwana are well known (Kroner et al. 1999; Collins et al. 2000; Yellappa and Rao 2018). The Pan-African Orogeny and its related magmatism and high-grade metamorphism are well established by several studies in Shillong Plateau (e.g. Ghosh et al. 2005; Chatterjee et al. 2007, 2011; Majumdar and Dutta 2016; Kumar et al. 2017). As discussed above, highly fractionated I-type granitoids of Nongpoh and Mylliem plutons related to mixing of mantle melts and lower and middle crust-derived melts, were emplaced at about 506.7 ± 7 Ma and Ca. 480–430 Ma respectively within Shillong Plateau in a post-collisional extension setting following the final amalgamation of east and west Gondwana blocks. Several workers have documented similar tectonics and extensional related origin of highly fractionated I-type granites (Wu et al. 2003a, b; Zhu et al. 2009; Huang et al. 2013; Zhou et al. 2016; Zhang et al. 2018). Granite plutons of Pan-African equivalents with geochemical characteristics similar to Nongpoh and Mylliem plutons in SP are well described in Arabian Nubian Shield, Brazilian shield and several parts of the world (Jackson et al. 1984; Eyal et al. 2004; Kroner and Stern 2004; Sami et al. 2017).

7 Conclusions

On the basis of field study, petrography, and whole-rock geochemical characteristics of the granitoids of Nongpoh and Mylliem plutons of Shillong Plateau, the conclusions derived on the genesis and evolution of the granitoids are summarized as:

1. Nongpoh and Mylliem plutons within Shillong Plateau in Northeast India consist of medium- to coarse-grained porphyritic quartz-monzonites (NQM) and granite (MG) emplaced at 506.7 ± 7 Ma and Ca. 480 to 430 Ma respectively in response to Pan-African orogeny.
2. Variation diagrams classify the NQM samples as high-K, alkali-calcic, metaluminous to weakly peraluminous granitoids and MG samples as high-K, alkali-calcic, weakly peraluminous granitoids.
3. Mineralogic, petrographic, and geochemical data demonstrate that the studied rocks are highly fractionated I-type granitoids, suggesting a significant mantle contribution which experienced fractional crystallization of several phases during magmatic evolution.
4. Parental magma for the granitoids was generated during a period of post-collisional extensional tectonic setting and thinning induced asthenosphere upwelling which triggered partial melting of mantle late in the cycle of Pan-African orogeny and subsequently evolved due to mixing of mantle-derived melts with crustal components of varied composition and fractional crystallization.
5. NQM evolved by partial melting of the lower crust while MG evolved by partial melting of the middle crust.

Acknowledgements The authors thank the editor and anonymous reviewers for the constructive reviews and suggestions which has enhanced the quality of the earlier version of the manuscript. They also thank the Head of Dept. of Earth Science, Assam University, Silchar, India for extending Laboratory facilities to carry out the

work. They are also thankful to the Directors of National Geophysical Research Institute, Hyderabad, India and NCESS Thiruvananthapuram, Kerala, India for the geochemical analysis. This research is financially supported by the Department of Science and Technology, Govt. of India under the Inspire Research Fellowship Programme (File No.: DST/Inspire Fellowship/2016/IF160812).

Compliance with ethical standards

Conflict of interest The corresponding author declares that there is no conflict of interest.

References

Abdel-Rahman AFM (2019) Geochemistry, age and origin of the Mons Claudianus TTG batholith (Egypt): insight into the role of Pan-African magmatism in uniting plates of Gondwana. Geol Mag 156(6):969–988

Avigad D, Gvirtzman Z (2009) Late Neoproterozoic rise and fall of the northern Arabian-Nubian shield: the role of lithospheric mantle delamination and subsequent thermal subsidence. Tectonophysics 477(3–4):217–228

Balaram V, Rao GT (2003) Rapid determination of REEs and other trace elements in geological samples by microwave acid digestion and ICP-MS. At Spectrosc 24:206–212

Barker F (1979) Trondhjemite: definition, environment and hypothesis of origin. In: Barker F (ed) Trondhjemites, dacites and related rocks. Elsevier, Amsterdam, pp 1–12

Batchelor AR, Bowden P (1985) Petrogenetic interpretation of granitoid rock series using multicationic parameter. Chem Geol 48:43–55

Bidyananda M, Deomurari MP (2007) Geochronological constraints on the evolution of Meghalaya massif, northeastern India: an ion microprobe study. Curr Sci 93:1620–1623

Chakrabarti R, Basu AR, Paul DK (2007) Nd–Hf–Sr–Pb isotopes and trace elementgeochemistry of Proterozoic lamproites from southern India: subducted komatiite in the source. Chem Geol 236(3–4):291–302

Chappell BW (1999) Aluminium saturation in I- and S-type granites and the characterization of fractionated haplogranites. Lithos 46:535–551

Chappell BW, White AJR (2001) Two contrasting granite types: 25 years later. Aust J Earth Sci 48:489–499

Chatterjee N (2017) Constraints from monazite and xenotime growth modelling in the MnCKFMASH-PYCe system on the P-T path of a metapelite from Shillong-Meghalaya Plateau: implications for the Indian shield assembly. J Metamorph Geol 35:393–412

Chatterjee N, Bhattacharya A, Duarah BP, Mazumdar AC (2011) Late Cambrian reworking of Palaeo-Mesoproterozoic granulites in Shillong-Meghalaya Gneissic Complex (Northeast India): evidence from PT pseudosection analysis and monazite chronology and implications for East Gondwana assembly. J Geol 119:311–330

Chatterjee N, Mazumdar AC, Bhattacharya A, Saikia RR (2007) Mesoproterozoic granulites of the Shillong-Meghalaya Plateau: evidence of westward continuation of the Prydz Bay Pan-African suture into Northeastern India. Precam Res 152:1–26

Chen CH, Lin W, Lu HY, Lee CY, Tien JL, Lai YH (2000) Cretaceous fractionated I-type granitoids and metaluminous A-type granites in SE China: the Late Yanshanian post-orogenic magmatism. Geol Soc Am Spec Pap 350:195–205

Chiaradia M (2009) Adakite-like magmas from fractional crystallization and melting-assimilation of mafic lower crust (Eocene Macuchi arc, Western Cordillera, Ecuador). Chem Geol 265:468–487

Choudhury DK, Pradhan AK, Zakaulla S, Umamaheswar K (2012) Geochemistry and petrogenesis of anorogenic (?) granitoids of west Garo Hills, Meghalaya. J Geol Soc India 80:276–286

Collins AS, Razakamanana T, Windley BF (2000) Neoproterozoic extensional detachment in central Madagascar: Implications for the collapse of the East African orogen. Geol Mag 137:39–51

Collins AS, Windley BF (2002) The tectonic evolution of central and northern Madagascar and its place in the final assembly of Gondwana. J Geol 110:325–340

Eyal M, Litvinovsky BA, Katzir Y, Zanvilevich AN (2004) The Pan-African high-K calc-alkaline peraluminous Elat granite from southern Israel: geology, geochemistry and petrogenesis. J Africa Earth Sci 40:115–136

Farahat ES, Zaki R, Hauzenberger C, Sami M (2011) Neoproterozoic calc-alkaline peraluminous granitoids of the Deleihimmi pluton, Central Eastern Desert, Egypt: implications for transition from late- to post-collisional tectonomagmatic evolution in the northern Arabian-Nubian Shield. Geol J 46(6):544–560

Frost BR, Barnes CG, Collins WJ, Arculus RJ, Ellis DJ, Frost CD (2001) A geochemical classification for granitic rocks. J Petrol 42:2033–2048

Ghatak A, Basu AR (2013) Isotopic and trace element geochemistry of alkalic–mafic–ultramafic–carbonatitic complexes and flood basalts in NE India: Origin in a heterogeneous Kerguelen plume. Geochim Cosmochim Acta 115:46–72

Ghosh S, Fallick AE, Paul DK, Potts PJ (2005) Geochemistry and origin of Neoproterozoic granitoids of Meghalaya, Northeast India: implication for linkage with amalgamation of Gondwana Supercontinent. Gond Res 8:421–432

Huang CM, Zhao ZD, Zhu DC, Liu D, Huang Y, Dung MC, Hu ZC, Zheng JP (2013) Geochemistry, zircon U–Pb chronology and Hf isotope of Luozha leucogranite, southern Tibet: implication for petrogenesis. Acta Petrol Sin 29:3689–3702

Jackson NJ, Walsh JN, Pegram E (1984) Geology, geochemistry and petrogenesis of late Precambrian granitoids in the Central Hijaz region of the Arabian Shield. Contrib Mineral Petrol 87:205–219

Kemp AIS, Wormald RJ, Whitehouse MJ, Price RC (2005) Hf isotopes in zircon reveal contrasting sources and crystallization histories for alkaline to peralkaline granites of Temora, south-eastern Australia. Geology 33:797–800

Kroner A, Hegner E, Collins AS, Windley BF, Brewer TS, Razakamanana T, Pidgeon RT (2000) Age and magmatic history of the Antananarivo Block, Central Madagascar, as derived from zircon geochronology and Nd isotope systematic. Am J Sci 330:251–258

Kroner A, Stern RJ (2004) Pan-African orogeny; Encyclopedia of Geology, vol 1. Elsevier, Amsterdam

Kroner A, Windley BF, Jaeckel P, Brewer TS, Razakamanana T (1999) New zircon ages and regional significance for the evolution of the Pan-African orogen in Madagascar. J Geol Soc London 156:1125–1135

Kumar S, Rino V, Hayasaka Y, Kimura K, Raju S, Terada K, Pathak M (2017) Contribution of Columbia and Gondwana Supercontinent assembly- and growth-related magmatism in the evolution of the Meghalaya Plateau and the Mikir Hills, Northeast India: constraints from U–Pb SHRIMP zircon geochronology and geochemistry. Lithos 277:356–375

Kumar GRR, Sreejith C (2016) Petrology and geochemistry of charnockites (felsic ortho-granulites) from the Kerala Khondalite Belt, Southern India: evidence for intra-crustal melting, magmatic differentiation and episodic crustal growth. Lithos 262:334–354

Li XH, Li ZX, Ge W, Zhou H, Li W, Liu Y, Wingate MTD (2003) Neoproterozoic granitoids in South China: crustal melting above a mantle plume at ca. 825 Ma? Precamb Res 122:45–83

Li XH, Li ZX, Li WX, Liu Y, Yuan C, Wei GJ, Qi CS (2007) U–Pb zircon, geochemical and Sr–Nd–Hf isotopic constraints on age and origin of Jurassic I- and A-type granites from central Guangdong, SE China: a major igneous event in response to foundering of a subducted flat-slab? Lithos 96(1–2):186–204

Li JW, Zhao XF, Zhou MF, Ma CQ, de Souza ZS, Vasconcelos P (2009) Late Mesozoic magmatism from the Daye region, eastern China: U–Pb ages, petrogenesis, and geodynamic implications. Contrib Miner Petrol 157:383–409

Majumdar D, Dutta P (2016) Geodynamic evolution of a Pan-African granitoid of extended Dizo Valley in Karbi Hills, NE India: Evidence from Geochemistry and Isotope Geology. J Asian Earth Sci 117:256–268

Meert JG (2003) A synopsis of events related to the assembly of eastern Gondwana. Tectonophysics 362(1–4):1–40

Meert JG, Van der Voo R (1997) The assembly of Gondwana 800–550 Ma. J Geodyn 23:223–236

Nandy DR (2001) Geodynamics of Northeastern India and the adjoining region. ACB Publication, Kolkata

O'Connor JT (1965) A classification for quartz-rich igneous rocks based on feldspar ratios. US Geoll Surv Prof Pap 525-B:79–84

Pearce JA (1996) Source and setting of granitic rocks. Episodes 19:120–125

Pearce JA, Harris NBW, Tindle AG (1984) Trace-element discrimination diagrams for the tectonic interpretation of granitic-rocks. J Petrol 25:956–983

Qiu JS, Xiao E, Hu J, Xu XS, Jiang SY, Li Z (2008) Petrogenesis of highly fractionated I-type granites in the coastal area of northeastern Fujian Province: constraints from zircon U–Pb geochronology, geochemistry, and Nd–Hf isotopes. Acta Petrol Sin 24(11):2468–2484

Ray JS, Pattanayak SK, Pande K (2005) Rapid emplacement of the Kerguelen plume-related Sylhet Traps, eastern India: Evidence from ^{40}Ar–^{39}Ar geochronology. Geophys Res Lett 32:1–4

Ray J, Saha A, Ganguly S, Balaram V, Krishna AK, Hazra S (2011) Geochemistry and petrogenesis of Neoproterozoic Mylliem granitoids, Meghalaya Plateau, northeastern India. J Earth Sys Sci 120(3):459–473

De la Roche H, Leterrier J, Grandclaude P, Marchal M (1980) A classification of volcanic and plutonic rocks using R1R2-diagram and major-element analyses—its relationships with current nomenclature. Chem Geol 29(1–4):183–210

Sadiq M, Umrao RK, Sharma BB, Chakraborti S, Bhattacharyya S, Kundu A (2018) Mineralogy, geochemistry and geochronology of mafic magmatic enclaves and their significance in evolution of Nongpoh granitoids, Meghalaya, NE India. Geol Soc Lond: Spec Publ 463:171–198

Sami M, Ntaflos T, Farahat ES, Mohamed HA, Ahmed AF, Hauzenberger C (2017) Mineralogical, geochemical and Sr–Nd isotopes characteristics of fluorite-bearing granites in the Northern Arabian-Nubian Shield, Egypt: Constraints on petrogenesis and evolution of their associated rare metal mineralization. Ore Geol Rev 88:1–22

Satyanarayanan M, Balaram V, Rao GT, Rajendra NP (2006) Application of ICP-MS in earth system sciences. J Geol Soc India 68:923–925

Srivastava RK, Sinha AK (2004) The early Cretaceous Sung Valley ultramafic–alkaline–carbonatite complex, Shillong Plateau, northeastern India: Petrological and genetic significance. Min Petrol 80:241–263

Streckeisen A (1976) To each plutonic rock its proper name. Earth Sci Rev 12:1–33

Streckeisen A, LeMaitre RW (1979) A chemical approximation to the modal QAPF classification of the igneous rocks. Neues Jahrb Mineral Abh 136:169–206

Sun SS, McDonough WF (1989) Chemical and isotopic systematics of oceanic basalts: implications for mantle composition and processes. In: Saunders AD, Norry MS (eds) Magmatism in ocean basins. Geological Society, London, Special Publications. vol 42, pp 313–345

Tao J, Li W, Li X, Cen T (2013) Petrogenesis of early Yanshanian highly evolved granites in the Longyuanba area, southern Jiangxi Province: evidence from zircon U–Pb dating, Hf–O isotope and whole-rock geochemistry. Sci China Earth Sci 56(6):922–939

Whalen JB, Curie KL, Chappell BW (1987) A-type granites: geochemical characteristics, discrimination and petrogenesis. Contrib Miner Petrol 95:407–419

Wolf MB, London D (1994) Apatite dissolution into peraluminous haplogranite melts: an experimental study of solubilities and mechanisms. Geochim Cosmochim Acta 58:4127–4145

Wu FY, Jahn BM, Wilde SA, Lo CH, Yui TF, Lin Q, Ge WC, Sun DY (2003a) Highly fractionated I-type granites in NE China (I): geochronology and petrogenesis. Lithos 66(3):241–273

Wu FY, Jahn BM, Wilde SA, Lo CH, Yui TF, Lin Q, Ge WC, Sun DY (2003b) Highly fractionated I-type granites in NE China (II): isotopic geochemistry and implications for crustal growth in the Phanerozoic. Lithos 67(3):191–204

Yellappa T, Rao JM (2018) Geochemical characteristics of Proterozoic granite magmatism from Southern Granulite Terrain, India: Implications for Gondwana. J Earth Sys Sci 127:22

Yin A, Dubey CS, Kelty TK, Webb AAG, Grove M, Gehrels GE, Burgess WP (2010) Geologic correlation of the Himalayan orogen and Indian Craton (Part 1): structural geology, U–Pb zircon geochronology, and tectonic evolution of the Shillong Plateau and its neighboring regions in NE India. Geol Soc Am Bull 122:336–359

Zhang Y, Cao H, Mo Xu, Zhang S, Li T, Wang S, Pei Q, Cai G, Shen T (2018) Petrogenesis of the late Mesozoic highly fractionated I-type granites in the Luanchuan district: implications for the tectono-magmatic evolution of eastern Qinling. Geosci J 22(2):253–272

Zhou Z, Ma C, Xie C, Wang L, Liu Y, Liu W (2016) Genesis of highly fractionated I-type granites from Fengshun Complex: implications to tectonic evolutions of South China. J Earth Sci 27(3):444–460

Zhu DC, Mo XX, Wang LQ, Zhao ZD, Niu YL, Zhou CY, Yang YH (2009) Petrogenesis of highly fractionated I-type granites in the Zayu area of eastern Gangdese, Tibet: constraints from zircon U–Pb geochronology, geochemistry and Sr–Nd–Hf isotopes. Sci China Ser D: Earth Sci 52(9):1223–1239